bilateral common carotid occlusion/stenosis [7]. Such background characteristics may have contributed to the successful modeling of carotid occlusive disease with infarcts in mice. Therefore, the current model differs from the BCAS model in terms of severity of histological changes because BCAS model induces white matter rarefaction but not infarcts while the current AC model is characterized by ischemic infarcts in the gray and white matter as a result of greater CBF reductions at later phase post-operation. Therefore, this model will be used to elucidate the mechanism of CBF autoregulation observed in humans and how this mechanism fails when systemic arterial pressure decreases below a critical point [16]. This would also be useful to investigate the dynamics of interstitial fluid and cerebrospinal fluid of the brain [17] as well as to test new therapeutic strategies for the large spectrum of neurological conditions associated with cerebral ischemia.

This study has a limitation in that the detailed mechanism of infarct formation remains unknown. In humans, cerebral infarctions distal to severe carotid artery diseases are caused by hemodynamic impairment and/or artery-to-artery embolism [1]. In the current mouse model without atheromatous lesions, although hemodynamic mechanism may be more plausible, detailed mechanisms remains unclear. Further analysis of the underlying mechanism of infarct formation in carotid artery occlusive disease can be conducted by using this novel animal model.

Another limitation is the relatively high mortality rate of the current model raising an issue of survival bias when future intervention study will be conducted with histological or behavioral assessment. However, since severe hemodynamic derangement itself seems to be a direct cause of mortality, death may become an endpoint and survival rate will be compared between the experimental groups to overcome the inherent limitation of the survival bias.

In summary, we have successfully established a mouse model of severe cerebrovascular insufficiency which almost invariably induce cerebral infarctions by placing ACs on the bilateral CCAs. We anticipate that pharmacological intervention for stroke will be investigated using this model by evaluation of survival rate, infarct formation, and CBF profile after the operation.

Acknowledgments

We thank Dr. Ahmad Khundakar for editing the manuscript and Prof. Hidenao Fukuyama for intellectual input. We are indebted to Ms. Takako Kawata for her excellent technical assistance in staining tissue sections.

Author Contributions

Conceived and designed the experiments: YH MI. Performed the experiments: YH. Analyzed the data: YH AK KN. Contributed reagents/materials/analysis tools: MI. Wrote the paper: YH MI.

References

1. Moustafa RR, Izquierdo-Garcia D, Jones PS, Graves MJ, Fryer TD, et al. (2010) Watershed infarcts in transient ischemic attack/minor stroke with > or = 50% carotid stenosis: hemodynamic or embolic? Stroke 41: 1410–1416.
2. Balestrini S, Perozzi C, Altamura C, Vernieri F, Luzzi S, et al. (2013) Severe carotid stenosis and impaired cerebral hemodynamics can influence cognitive deterioration. Neurology 80: 2145–2150.
3. Lai SL, Chen YC, Weng HH, Chen ST, Hsu SP, et al. (2005) Bilateral common carotid artery occlusion–a case report and literature review. J Neurol Sci 238: 101–104.
4. AbuRahma AF, Copeland SE (1998) Bilateral internal carotid artery occlusion: natural history and surgical alternatives. Cardiovasc Surg 6: 579–583.
5. Jiwa NS, Garrard P, Hainsworth AH (2010) Experimental models of vascular dementia and vascular cognitive impairment: a systematic review. J Neurochem 115: 814–828.
6. Hattori H, Takeda M, Kudo T, Nishimura T, Hashimoto S (1992) Cumulative white matter changes in the gerbil brain under chronic cerebral hypoperfusion. Acta Neuropathol 84: 437–442.
7. Kitagawa K, Matsumoto M, Yang G, Mabuchi T, Yagita Y, et al. (1998) Cerebral ischemia after bilateral carotid artery occlusion and intraluminal suture occlusion in mice: evaluation of the patency of the posterior communicating artery. J Cereb Blood Flow Metab 18: 570–579.
8. Herrmann M, Stern M, Vollenweider F, Nitsch C (2004) Effect of inherent epileptic seizures on brain injury after transient cerebral ischemia in Mongolian gerbils. Exp Brain Res 154: 176–182.
9. Yang G, Kitagawa K, Matsushita K, Mabuchi T, Yagita Y, et al. (1997) C57BL/6 strain is most susceptible to cerebral ischemia following bilateral common carotid occlusion among seven mouse strains: selective neuronal death in the murine transient forebrain ischemia. Brain Res 752: 209–218.
10. Kitamura A, Fujita Y, Oishi N, Kalaria RN, Washida K, et al. (2012) Selective white matter abnormalities in a novel rat model of vascular dementia. Neurobiol Aging 33: 1012 e1025–1035.
11. Shibata M, Ohtani R, Ihara M, Tomimoto H (2004) White matter lesions and glial activation in a novel mouse model of chronic cerebral hypoperfusion. Stroke 35: 2598–2603.
12. Ayata C, Dunn AK, Gursoy OY, Huang Z, Boas DA, et al. (2004) Laser speckle flowmetry for the study of cerebrovascular physiology in normal and ischemic mouse cortex. J Cereb Blood Flow Metab 24: 744–755.
13. Forrester KR, Stewart C, Tulip J, Leonard C, Bray RC (2002) Comparison of laser speckle and laser Doppler perfusion imaging: measurement in human skin and rabbit articular tissue. Med Biol Eng Comput 40: 687–697.
14. Shibata M, Yamasaki N, Miyakawa T, Kalaria RN, Fujita Y, et al. (2007) Selective impairment of working memory in a mouse model of chronic cerebral hypoperfusion. Stroke 38: 2826–2832.
15. Bink DI, Ritz K, Aronica E, van der Weerd L, Daemen MJ (2013) Mouse models to study the effect of cardiovascular risk factors on brain structure and cognition. J Cereb Blood Flow Metab 33: 1666–1684.
16. Willie CK, Tzeng YC, Fisher JA, Ainslie PN (2014) Integrative regulation of human brain blood flow. J Physiol 592: 841–859.
17. Carare RO, Hawkes CA, Jeffery M, Kalaria RN, Weller RO (2013) Review: cerebral amyloid angiopathy, prion angiopathy, CADASIL and the spectrum of protein elimination failure angiopathies (PEFA) in neurodegenerative disease with a focus on therapy. Neuropathol Appl Neurobiol 39: 593–611.

Chapter 8

A Mouse Model of Chronic Cerebral Hypoperfusion Characterizing Features of Vascular Cognitive Impairment

Masafumi Ihara, Akihiko Taguchi, Takakuni Maki, Kazuo Washida, and Hidekazu Tomimoto

Abstract

Vascular dementia or vascular cognitive impairment occurs as a result of persistently compromised blood flow to the brain and represents the second most common type of dementia after Alzheimer's disease. In order to investigate its underlying mechanisms, a mouse model of chronic cerebral hypoperfusion has been developed, which involves the narrowing of the bilateral common carotid arteries with newly designed microcoils. This mouse model provides a unique platform to investigate the mechanisms of angiogenesis following chronic cerebral hypoperfusion and to explore potential drugs or cell therapies designed to enhance angiogenesis as a preclinical step toward developing novel treatments for dementia of vascular origin.

Key words Chronic cerebral hypoperfusion, Vascular cognitive impairment, Dementia, Bilateral common carotid artery occlusion, Microcoil, Mouse, Cerebral blood flow, Laser speckle flowmetry

1 Introduction

Cerebral blood flow (CBF) is decreased diffusely, or at least focally, in elderly patients with vascular cognitive impairment [1, 2]. To mimic such persistent cerebral ischemia in humans, a chronic cerebral hypoperfusion model has been established in rats, gerbils, and mice [3–5]. The model can be generated by bilateral common carotid artery (CCA) occlusion in rats [3, 6], bilateral CCA stenosis in mice (BCAS) [4, 7–9] or in gerbils [5], and unilateral CCA occlusion in mice [10]. Although nonhuman primates appear to represent the best model for the study of vascular cognitive impairment, due to their similarities in cerebral vascular architectures with humans [11], most experiments studying chronic cerebral hypoperfusion have been performed in rodents because of the ease of handling and greater ethical acceptability.

Among rodent models of chronic cerebral hypoperfusion, the rat model is most widely used [12, 13], resulting in cognitive impairment and cholinergic deficits in the animal [3, 6, 14].

Richard Milner (ed.), *Cerebral Angiogenesis: Methods and Protocols*, Methods in Molecular Biology, vol. 1135,
DOI 10.1007/978-1-4939-0320-7_8,

The animals also develop white matter rarefaction [3, 9, 15], which appears very similar to that found in human cerebrovascular white matter lesions. However, the rat model does possess inherent drawbacks. For example, the visual pathway is invariably damaged by the occlusion of the ophthalmic arteries, thus potentially compromising behavioral assessment. Furthermore, genetic studies may be hampered because of limited accessibility to molecular technologies in the rat.

To circumvent such limitations, we have established a mouse model of chronic cerebral hypoperfusion, which is subjected to various degrees of CBF reduction by the narrowing of the bilateral CCAs with newly designed microcoils [4, 7–9]. The severity of ischemia/hypoperfusion can be easily controlled by internal diameter regulation of the microcoils [4]. The model demonstrates good reproducibility in terms of glial activation, blood–brain barrier disruption, white matter lesion appearance, and vascular cognitive impairment, which appear within a month after the surgery. In the longer-term model, significant hippocampal changes (atrophy and cell death) are documented 8 months after surgery, providing evidence linking chronic cerebral hypoperfusion with neurodegeneration [16]. The apparent advantage of using this surgical technique is that it provides a unique platform to investigate the mechanisms of angiogenesis and to explore potential drugs [17, 18] or cell therapies [19] designed to enhance angiogenesis as a preclinical step toward developing novel treatments for dementia of vascular origin. Another important advantage is its easy application to genetically engineered mice; for instance, β amyloid-overexpressing mice have been subjected to BCAS to clarify the wider question of whether and how chronic cerebral hypoperfusion has detrimental effects on Alzheimer's disease [20–22].

The aims of the current chapter are therefore to provide technical details that have accumulated since establishment of this mouse BCAS model, focusing particularly on a method of CBF monitoring using laser speckle flowmetry in order to consider the particular strengths and pitfalls of the method.

2 Materials

2.1 Animals and Surgical Appliances

1. Male C57BL/6J mice (weight, 24–29 g) (*see* **Note 1**).
2. Animal restraining device.
3. Heating pad.
4. Rectal thermometer.
5. Chemical depilatory.
6. Surgical scrub solutions: povidone-iodine scrub (Betadine scrub) or chlorhexidine scrub.

7. Anesthetics: halothane or isoflurane (*see* **Note 2**).
8. Surgical knife.
9. Silk suture.
10. Forceps: fine-tip and blunt-tip forceps.
11. Gauze.
12. Stainless steel wound clips.
13. Microcoils: manufactured in the Sawane Spring Co., Ltd. (Hamamatsu, Japan) (*see* **Note 3**).
14. Operating microscope.

2.2 CBF Monitoring Device

1. Laser speckle blood flow imager (Omegawave, Inc., Tokyo, Japan).
2. A calibration reference device (Calibrator S/N 080715-5, Omegawave, Inc.)
3. Gel (Aquasonic, Parker Laboratories, Inc., Fairfield, NJ).

3 Methods

Before performing surgery, one should be aware that there are legal and ethical requirements regarding the use of animals in research. The animal must be maintained in a surgical plane of anesthesia, and its vital signs monitored and regulated throughout the procedure.

3.1 Surgical Procedures

1. Anesthetize the mouse with gas anesthetics (*see* **Note 4**).
2. Place the anesthetized mouse in a dorsal recumbent position on the operating board with the tail toward the surgeon.
3. Shave the ventral neck area with a chemical depilatory and swab with surgical scrub.
4. Make a 1.0–1.5 cm midline skin incision from the base of the neck to the point below the lower jaw.
5. Remove the underlying fat and move the salivary glands laterally or upwards using forceps to maximize the operating field.
6. Expose and free both common carotid arteries (CCAs) from their sheaths under an operating microscope (*see* **Note 5**) (Fig. 1).
7. Place two 4–0 silk sutures around the distal and proximal parts of the CCA.
8. Gently lift the artery by the sutures and place between the loops of the microcoil just proximal to the carotid bifurcation (Fig. 1) (*see* **Note 6**).
9. Twine the microcoil by rotating it around the CCA (*see* **Note 7**).
10. 30 min later, twine another microcoil of the same size around the other CCA (Fig. 1) (*see* **Note 8**).

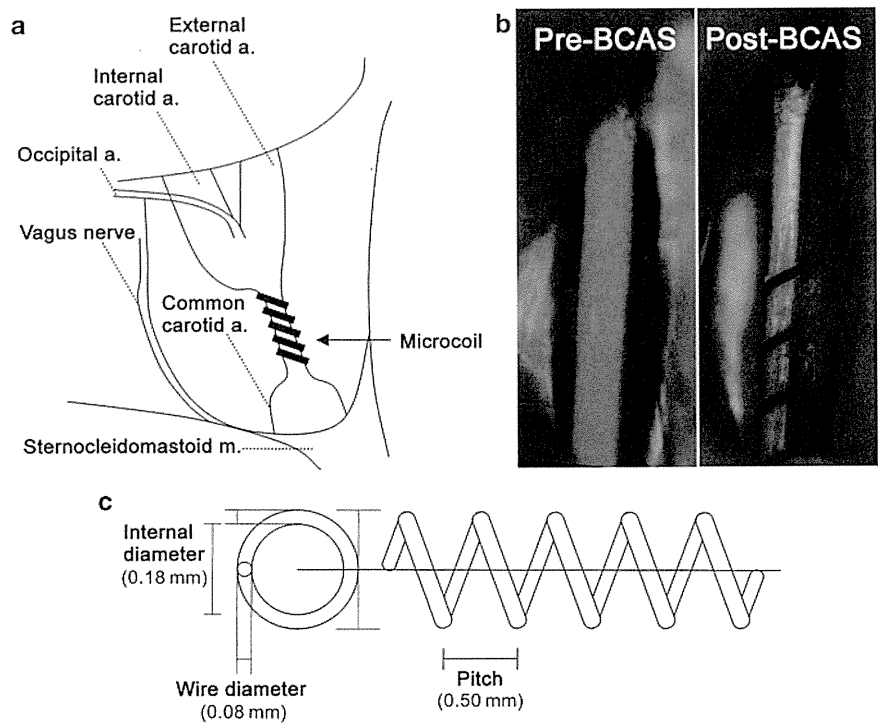

Fig. 1 The procedure for BCAS and microcoil placement. The microcoil is twined by rotating it around the CCA just proximal to the carotid bifurcation of a C57BL/6J mouse (**a**). Representative photographs of a FITC-perfused common carotid artery before (*left*) and after (*right*) placement of a microcoil (**b**). The most frequently used microcoil is made from piano wire (wire diameter of 0.08 mm) with an inner diameter of 0.18 mm, pitch 0.50 mm, and total length 2.5 mm (**c**)

11. Close the incision with stainless steel wound clips or fine sutures.
12. Return the mouse to the animal holding area after they appear normal (*see* **Note 9**).

3.2 Cerebral Blood Flow (CBF) Monitoring

1. Place the anesthetized mouse in a ventral recumbent position with the tail toward the surgeon (*see* **Note 4**).
2. Surgically remove the scalp to expose the skull.
3. Using fine-tip forceps, remove the periosteum, which adheres to the skull (*see* **Note 10**).
4. Wipe the skull surface with saline-soaked gauze and then cover with a thin layer of gel to prevent drying (*see* **Note 11**).
5. Perform calibration with a calibration reference device (*see* **Note 12**).
6. Perform CBF recordings through the skull using the laser speckle blood flow imager, (*see* **Note 13**) (Fig. 2). Define circular regions of interest on the image for quantitative measurement (*see* **Note 14**).

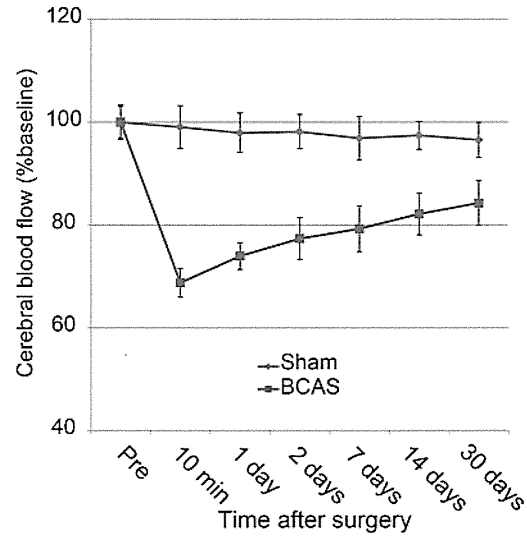

Fig. 2 Cerebral blood flow after BCAS. This figure shows temporal profiles of cerebral blood flow evaluated with laser speckle imager in mice at 2.5 months of age after the surgery using microcoils with diameter of 0.18 mm (*square*) and in sham-operated mice (*diamond*). The data represent mean values ± standard deviation expressed as a percentage of the preoperative value. The CBF values decreased significantly from the preoperative baseline after the surgery with the 0.18 mm diameter microcoils. Immediately after surgery (10 min), there was a significant reduction in CBF values to 68.8 ± 2.8 %, with gradual recovery to 84.3 ± 4.3 % at 1 month ($n=7$), probably due to compensatory mechanisms involving angiogenesis and arteriogenesis [4, 17]. Note that the CBF values, as a percentage of the preoperative value in the sham-operated mice ($n=7$), tended to decrease, although not significantly, probably as a result of minimal fibrous scar tissue build up and bone opacification regardless of appropriate treatment (*see* **Note 10**)

4 Notes

1. This model should be applied exclusively to the C57BL/6J strain, as CBF in other strains may have a greater variability after BCAS [4, 8, 23].
2. Although anesthetics are known to provide varying degrees of neuroprotection against ischemic injury, the selection of anesthesia did not appreciably affect the mortality rates, temporal profile of CBF, and ischemic white matter changes after BCAS.
3. Four types of microcoils are made from piano wire with varying inner diameters from 0.16 mm to 0.22 mm. Researchers in Japan may obtain the microcoils directly from the manufacturer (Sawane Spring Co., Ltd, Hamamatsu, Japan), but those outside Japan may purchase the microcoils from Invitrotech Co., Ltd. (Kyoto, Japan). The microcoils should be thoroughly disinfected with alcohol and air dried just before use.

4. Anesthesia is usually induced with 4 % isoflurane and maintained with 1.5 % isoflurane, via a face mask. Alternatively, halothane may be used with 4 % for induction and 1.5 % for maintenance.
5. Separate the carotid from the vagus nerve, which is a white, string-like object directly lateral to the carotid artery. Particular care should be taken to avoid damage to the vagus nerve.
6. Cessation of CBF for >1 min should be avoided.
7. For this manipulative procedure, one should avoid piercing the artery with either end of the microcoil. Instead of rotating the microcoil around the CCA, one may alternatively wind the artery along the groove of the coil.
8. In our original report, we used 30 min intervals between manipulations on the left and right CCAs to avoid early mortality [4]. However, no intervals may be required to generate this model. During the surgery, rectal temperature should be maintained between 36.5 °C and 37.5 °C.
9. The mortality rates range from 3 % to 5 % in mice with microcoils of 0.18 mm in diameter (unpublished data), although earlier studies suggested higher mortality rates, 13 % in mice with microcoils of 0.22 mm in diameter, 17 % in those of 0.20 mm, and 15–19 % in those of 0.18 mm [4, 24]. In contrast, 75 % (15/20) of mice with microcoils of 0.16 mm diameter administered died within 14 days after the surgery, most of whom were found to have cerebral infarctions [4]. In another study of a modified model with a 0.16 mm microcoil placed on the left CCA and the 0.18 mm microcoil on the right CCA, the mortality rate is reported to be 18.8 % [25].
10. It is important to remove the periosteum, which adheres tightly to the skull, with fine-tip forceps to minimize fibrous scar tissue buildup without significant changes in flow signals in sham-operated mice [19]. Swabbing the skull surface should be done gently. Rough or inappropriate treatment leads to scar tissue build up along the cranial sutures. It is difficult to reverse fibrous scar tissue buildup and bone opacification. If they do occur, another animal should be used for the experiment. Although most bleeding stops spontaneously, the wound should be checked postoperatively for blood stains on the skull, which, if present, must be removed gently with saline-soaked gauze.
11. For each recording, the skull surface should be wiped with saline-soaked gauze, covered with a thin layer of gel (Aquasonic, Parker Laboratories, Inc.), and immersed for 5–10 min. Care should be taken to ensure the surface is fully wet as indicated by a semitransparent appearance. A dry surface, as indicated by a white skull, or a partially wet surface results in a reduction in flow signal intensity.

12. Laser speckle imaging requires a baseline to anchor for repetitive measurement or comparison between different subjects. We use a calibration reference device (Calibrator S/N 080715-5, Omegawave, Inc.) and assign a value to this reference material (arbitrarily assigned value, 25.0). The value is attributed to the Brownian motion of red-colored particles (0.35 μm, 24 °C). Calibration with this device before each test provides standardized values for comparison.
13. CBF should be measured after CBF is stabilized after anesthesia. During the CBF recordings, the rectal temperature should be maintained between 36.5 °C and 37.5 °C. One can successfully image through the skull repeatedly up to 30 days after the operation [17, 19, 26]. Success is mostly dependent on the degree of removal of the periosteum.
14. It is ideal to measure the mean CBF in identically sized regions of interest (900 pixels) located 1 mm posterior and 2 mm lateral from the bregma.

Acknowledgement

We would like to express our gratitude to Dr. Ahmad Khundakar for insightful comments and editing. We would also like to thank Dr. Shibata, Dr. Nakaji, Dr. Fujita, Dr. Nishio, and Dr. Yamada (former members of Kyoto University) who have been involved in the establishment, characterization, and optimization of this animal model. This work was partially supported by Banyu Life Science Foundation International and was also supported by the Grant-in-Aid for Scientific Research (B) (M.I. No. 23390233) and by the Grant-in-Aid from the Ministry of Health, Labour and Welfare of Japan (M.I. No. 2450101-001).

References

1. Ihara M, Tomimoto H, Ishizu K et al (2004) Decrease in cortical benzodiazepine receptors in symptomatic patients with leukoaraiosis: a positron emission tomography study. Stroke 35:942–947
2. Yao H, Sadoshima S, Kuwabara Y et al (1990) Cerebral blood flow and oxygen metabolism in patients with vascular dementia of the Binswanger type. Stroke 21:1694–1699
3. Wakita H, Tomimoto H, Akiguchi I et al (1994) Glial activation and white matter changes in the rat brain induced by chronic cerebral hypoperfusion: an immunohistochemical study. Acta Neuropathol 87:484–492
4. Shibata M, Ohtani R, Ihara M et al (2004) White matter lesions and glial activation in a novel mouse model of chronic cerebral hypoperfusion. Stroke 35:2598–2603
5. Kudo T, Tada K, Takeda M et al (1990) Learning impairment and microtubule-associated protein 2 decrease in gerbils under chronic cerebral hypoperfusion. Stroke 21: 1205–1209
6. Sarti C, Pantoni L, Bartolini L et al (2002) Persistent impairment of gait performances and working memory after bilateral common carotid artery occlusion in the adult Wistar rat. Behav Brain Res 136:13–20
7. Ihara M, Tomimoto H (2011) Lessons from a mouse model characterizing features of vascular cognitive impairment with white matter changes. J Aging Res 2011:978761

8. Shibata M, Yamasaki N, Miyakawa T et al (2007) Selective impairment of working memory in a mouse model of chronic cerebral hypoperfusion. Stroke 38:2826–2832
9. Coltman R, Spain A, Tsenkina Y et al (2011) Selective white matter pathology induces a specific impairment in spatial working memory. Neurobiol Aging 32:2324.e7–12
10. Yoshizaki K, Adachi K, Kataoka S et al (2008) Chronic cerebral hypoperfusion induced by right unilateral common carotid artery occlusion causes delayed white matter lesions and cognitive impairment in adult mice. Exp Neurol 210:585–591
11. Stroke Therapy Academic Industry Roundtable (STAIR) (1999) Recommendations for standards regarding preclinical neuroprotective and restorative drug development. Stroke 30: 2752–2758
12. Farkas E, Luiten PG, Bari F (2007) Permanent, bilateral common carotid artery occlusion in the rat: a model for chronic cerebral hypoperfusion-related neurodegenerative diseases. Brain Res Rev 54:162–180
13. Jiwa NS, Garrard P, Hainsworth AH (2010) Experimental models of vascular dementia and vascular cognitive impairment: a systematic review. J Neurochem 115:814–828
14. Ni JW, Matsumoto K, Li HB et al (1995) Neuronal damage and decrease of central acetylcholine level following permanent occlusion of bilateral common carotid arteries in rat. Brain Res 673:290–296
15. Holland PR, Bastin ME, Jansen MA et al (2011) MRI is a sensitive marker of subtle white matter pathology in hypoperfused mice. Neurobiol Aging 32:2325.e1–6
16. Nishio K, Ihara M, Yamasaki N et al (2010) A mouse model characterizing features of vascular dementia with hippocampal atrophy. Stroke 41:1278–1284
17. Maki T, Ihara M, Fujita Y et al (2011) Angiogenic and vasoprotective effects of adrenomedullin on prevention of cognitive decline after chronic cerebral hypoperfusion in mice. Stroke 42:1122–1128
18. Maki T, Ihara M, Fujita Y et al (2011) Angiogenic roles of adrenomedullin through vascular endothelial growth factor induction. Neuroreport 22:442–447
19. Fujita Y, Ihara M, Ushiki T et al (2010) Early protective effect of bone marrow mononuclear cells against ischemic white matter damage through augmentation of cerebral blood flow. Stroke 41:2938–2943
20. Kalaria RN, Akinyemi R, Ihara M (2012) Does vascular pathology contribute to Alzheimer changes? J Neurol Sci 322(1–2):141–147
21. Okamoto Y, Yamamoto T, Kalaria RN et al (2012) Cerebral hypoperfusion accelerates cerebral amyloid angiopathy and promotes cortical microinfarcts. Acta Neuropathol 123:381–394
22. Yamada M, Ihara M, Okamoto Y et al (2011) The influence of chronic cerebral hypoperfusion on cognitive function and amyloid β metabolism in APP overexpressing mice. PloS One 6:e16567
23. Nakaji K, Ihara M, Takahashi C et al (2006) Matrix metalloproteinase-2 plays a critical role in the pathogenesis of white matter lesions after chronic cerebral hypoperfusion in rodents. Stroke 37:2816–2823
24. Duan W, Gui L, Zhou Z et al (2009) Adenosine A2A receptor deficiency exacerbates white matter lesions and cognitive deficits induced by chronic cerebral hypoperfusion in mice. J Neurol Sci 285:39–45
25. Miki K, Ishibashi S, Sun L et al (2009) Intensity of chronic cerebral hypoperfusion determines white/gray matter injury and cognitive/motor dysfunction in mice. J Neurosci Res 87:1270–1281
26. Washida K, Ihara M, Nishio K et al (2010) Nonhypotensive dose of telmisartan attenuates cognitive impairment partially due to peroxisome proliferator-activated receptor-gamma activation in mice with chronic cerebral hypoperfusion. Stroke 41:1798–1806

ELSEVIER

Neurobiology of Aging 33 (2012) 1012.e25–1012.e35

NEUROBIOLOGY OF AGING

www.elsevier.com/locate/neuaging

Selective white matter abnormalities in a novel rat model of vascular dementia

Akihiro Kitamura[a], Youshi Fujita[a], Naoya Oishi[b], Raj N. Kalaria[c], Kazuo Washida[a], Takakuni Maki[a], Yoko Okamoto[a], Yoshiki Hase[a], Mahito Yamada[a], Jun Takahashi[d], Hidefumi Ito[a], Hidekazu Tomimoto[e], Hidenao Fukuyama[b], Ryosuke Takahashi[a], Masafumi Ihara[a,*]

[a] *Department of Neurology, Graduate School of Medicine, Kyoto University, Sakyo-ku, Kyoto, Japan*
[b] *Human Brain Research Center, Graduate School of Medicine, Kyoto University, Kyoto, Japan*
[c] *Institute for Ageing and Health, WRC, Campus for Ageing and Vitality, Newcastle University, Newcastle, UK*
[d] *Department of Biological Repair, Institute for Frontier Medical Sciences, Kyoto University, Kyoto, Japan*
[e] *Department of Neurology, Graduate School of Medicine, Mie University, Tsu, Japan*

Received 17 August 2011; received in revised form 25 October 2011; accepted 26 October 2011

Abstract

Rats subjected to bilateral common carotid artery (CCA) occlusion or 2-vessel occlusion (2VO) have been used as animal models of subcortical ischemic vascular dementia. However, this model possesses an inherent limitation in that cerebral blood flow (CBF) drops too sharply and substantially after ligation of CCAs. To circumvent such hypoxic-ischemic conditions, we tested implantation of the ameroid constrictor device on bilateral CCAs of male Wistar-Kyoto rats and more precisely replicated chronic cerebral hypoperfusion by gradual narrowing of the CCAs (2-vessel gradual occlusion; 2VGO). The acute cerebral blood flow reduction and resultant inflammatory responses observed in the 2VO rats were eliminated in the 2VGO rats. Thus, chronic cerebral hypoperfusion was segregated, and induced selective white matter changes with relatively preserved neurovascular coupling and substantially less metabolic and histological derangements in the gray matter including the hippocampus. This led to significant spatial working memory impairment of a magnitude similar to the 2VO rats at 28 days postoperation. The 2VGO model may more closely mimic cognitive impairment subsequent to selective white matter damage.

Keywords: Vascular dementia; Chronic cerebral hypoperfusion; Ameroid constrictor; White matter change; Rat; Neurovascular coupling

1. Introduction

Vascular dementia (VaD) is the second most common cause of dementing illnesses after Alzheimer's disease (AD). Approximately half of all cases of vascular dementia are explained by subcortical ischemic vascular dementia (SIVD) (Yoshitake et al., 1995), which is characterized by lacunar infarctions in the basal ganglia and ischemic white matter changes. Loss of vasomotor reactivity in the small vessels and resultant chronic cerebral hypoperfusion with blood-brain barrier (BBB) disruption and glial activation may underlie the white matter changes (Marshall and Lazar, 2011; Pantoni, 2010).

To mimic such a pathological condition and explore the underlying mechanisms, several animal models of chronic cerebral hypoperfusion have been developed, including bilateral common carotid artery (CCA) or 2-vessel occlusion (2VO) in rats, bilateral CCA stenosis in gerbils or mice (BCAS) (Shibata et al., 2004), and unilateral CCA occlusion in mice (Yoshizaki et al., 2008). Among these, the rat 2VO model has been frequently used (Jiwa et al., 2010) and may become more important when genetically-modified rats

* Corresponding author at: Kyoto University, 54 Kawahara-cho, Shogoin, Sakyo, Kyoto 606-8507, Japan. Tel.: +81 75 751 3766; fax: +81 75 751 3265.
E-mail address: ihara@kuhp.kyoto-u.ac.jp (M. Ihara).

0197-4580/$ – see front matter © 2012 Elsevier Inc. All rights reserved.
doi:10.1016/j.neurobiolaging.2011.10.033

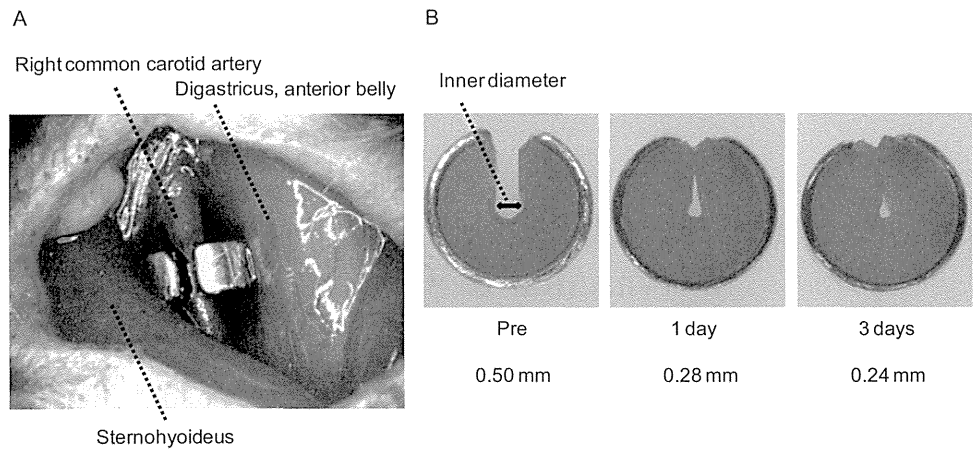

C

	Pre	1 day	3 days
Inner diameter (mm)	0.500±0.000	0.282±0.00259	0.241±0.00239
range (mm)	0.500-0.500	0.271-0.293	0.235-0.245

Data are the mean±SEM.

Fig. 1. (A) Surgical implantation of the ameroid constrictor device on the right common carotid artery. (B) Representative images of ameroid constrictors at indicated time points. (C) Table showing the temporal profiles of stenosis of ameroid constrictor before surgical implantation (n = 4), and 1 (n = 8) and 3 days (n = 4) postoperation.

are widely available. The 2VO model exhibits characteristic features of SIVD, such as white matter damage (Wakita et al., 1994, 2002), and cognitive impairment (Farkas et al., 2007; Hainsworth and Markus, 2008; Jiwa et al., 2010). Nevertheless, this model possesses an inherent limitation in that cerebral blood flow (CBF) drops too sharply and substantially after the ligation of the CCAs and remains too low (30%–45% of the baseline level) for 2–3 days; this therefore creates hypoxic-ischemic conditions too severe to replicate "chronic" cerebral hypoperfusion (Marosi et al., 2006). After this acute phase, CBF gradually recovers but still remains relatively low (50%–90%) for 8 weeks to 3 months postoperation (chronic phase) (Otori et al., 2003; Tomimoto et al., 2003). Although the sustained oligemia in the chronic phase is believed to better replicate chronic cerebral hypoperfusion associated with SIVD, the contribution of the preceding acute phase to the neuropathological and behavioral consequences is an ongoing concern (Farkas et al., 2007). We therefore sought to establish a novel rat model that eliminates the acute phase, meaning that CBF would gradually decrease to the level in the chronic phase, using the ameroid constrictor device. This device could predictably achieve gradual narrowing of the CCAs and establish a rat model of SIVD that replicates "chronic" cerebral hypoperfusion more precisely. We therefore henceforth refer to this novel rat model as the "2-vessel gradual occlusion (2VGO)" model.

2. Methods

2.1. Animals

We used 12- to 14-week-old male Wistar-Kyoto rats (WKY) (See Supplemental Method I for details).

2.2. Ameroid constrictor

The ameroid constrictor (Research Instruments NW, Lebanon, OR, USA) consists of a stainless steel casing surrounding a hygroscopic casein material that has an internal lumen. The casein component gradually absorbs water and consequently swells, leading to predictable narrowing and occlusion of the arterial lumen that it encases (Fig. 1). The inner diameter was 0.5 mm, the outer diameter 3.25 mm, and the length 1.28 mm.

2.3. Study design

WKY rats were divided into 3 groups: 2-vessel gradual occlusion (2VGO), 2-vessel occlusion (2VO), and sham control groups (Supplemental Method II). Temporal changes of blood flow in the CCAs were recorded by computed tomography-angiography (CTA); the CBF in the frontal cortices was measured by laser speckle flowmetry (LSF; Omega, Zone; Omegawave, Tokyo, Japan), and ^{18}F-fluorodeoxyglucose (FDG) positron emission tomography (PET) imaging was performed at indicated time points. Histologic evaluation of demyelinating changes

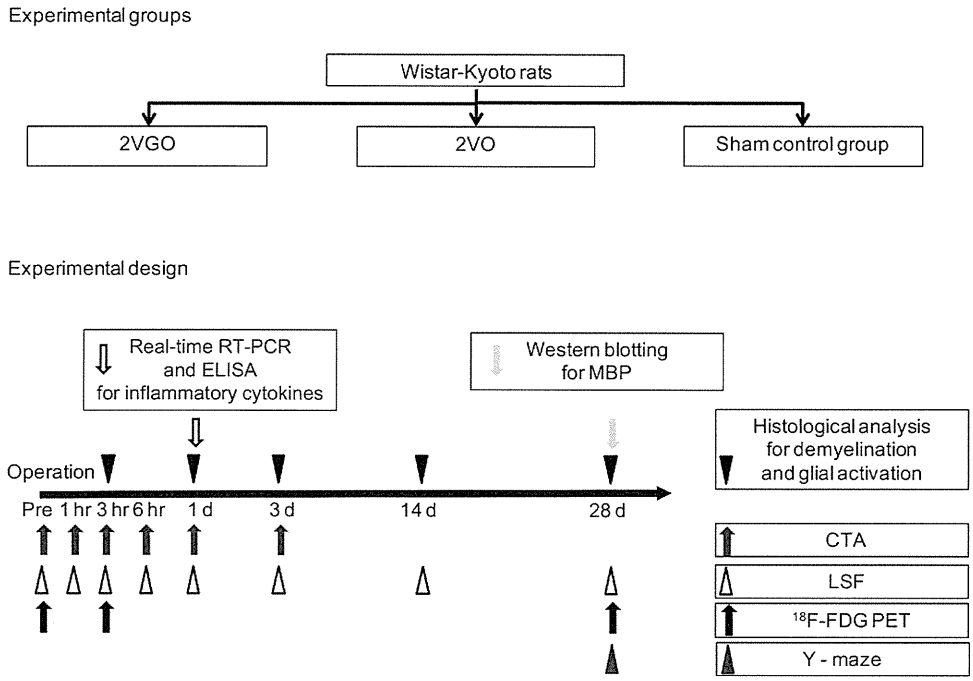

Fig. 2. Experimental protocol. Abbreviations: d, day; hr, hour.

and glial activation, analysis of cerebral messenger RNA (mRNA) and protein levels of inflammatory cytokines and Western blotting analysis of myelin basic protein (MBP) were performed at indicated points. Spatial working memory was assessed by the Y-maze test (Fig. 2).

2.4. Surgical procedure

Under anesthesia, the 2VGO rats were subjected to surgical implantation of ameroid constrictors on the CCAs bilaterally whereas in the 2VO group, both the CCAs were ligated (Supplemental Method III).

2.5. Computed tomography-angiography

CTA of the bilateral CCAs was repeatedly performed under anesthesia using the R_mCT system (Rigaku, Tokyo, Japan) (Supplemental Method IV).

2.6. Cerebral blood flow, blood pressure, and pulse rate measurement

CBF in the frontal cortices was recorded by LSF under anesthesia with isoflurane, 1.5% (Supplemental Method V).

2.7. ^{18}F-FDG PET acquisition and image analysis

Small animal PET imaging was performed to assess temporal changes in ^{18}F-FDG uptake during the first 5 minutes and again between 45 and 90 minutes (Supplemental Method VI).

2.8. Histologic evaluation of demyelinating changes and glial activation

Paraffin-embedded coronal sections of the brain (6 μm thick) were analyzed with hematoxylin-eosin (HE) staining for detection of infarcted areas in the forebrain and for neurodegeneration in the hippocampal CA1 and CA3 regions, and with Klüver-Barrera staining for demyelinating changes. The severity of the white matter lesions in the optic chiasma, medial and lateral parts of the corpus callosum, and caudoputamen, was graded as normal (grade 0), disarrangement of the nerve fibers (grade 1), the formation of marked vacuoles (grade 2), and the disappearance of myelinated fibers (grade 3), according to the established criteria (Wakita et al., 1994). They were also immunostained for ionized calcium binding adapter molecule-1 (Iba-1; a marker of microglia; Wako, Osaka, Japan), glial fibrillary acidic protein (GFAP; astrocyte; Dako, Glostrup, Denmark), glutathione *S*-transferase-π (GST-π; oligodendrocyte; Assay Designs, Ann Arbor, MI, USA), degraded MBP (dMBP; demyelinating changes; a gift from Dr. Wakita) (Ihara et al., 2010), and myelin-associated glycoprotein (MAG; Santa Cruz Biotechnology, CA, USA) (Supplemental Method VII).

2.9. Quantitative real-time reverse transcriptase-polymerase chain reaction (RT-PCR)

Cerebral mRNA levels of the monocyte chemoattractant protein-1 (MCP-1) and tumor necrosis factor-α (TNF-α)

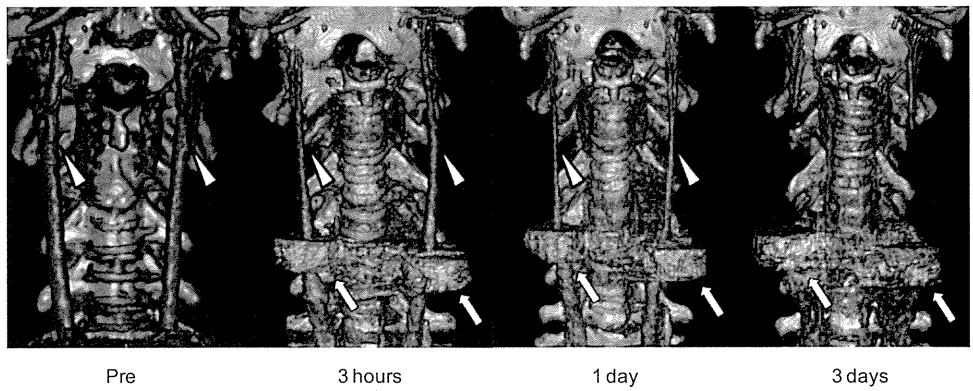

Fig. 3. Three-dimensional volume-rendered images of computed tomography (CT)-angiography showing the blood flow of the bilateral common carotid arteries pre- and postimplantation of ameroid constrictors at indicated time intervals. Arrowheads indicate common carotid arteries and arrows ameroid constrictors.

were assessed by quantitative real-time RT-PCR (Supplemental Method VIII).

2.10. Enzyme-linked immunosorbent assay (ELISA) for TNF-α

The protein concentration of TNF-α in brain homogenates were also measured using a specific ELISA kit according to the manufacturer's recommendation (R&D Systems, Minneapolis, MN, USA) (Supplemental Method IX).

2.11. Western blotting analysis for myelin basic protein

The optic nerves and chiasma were analyzed for demyelinating changes. A rabbit anti-MBP antibody and a mouse anti β-actin antibody (which served as an internal control), were used (Supplemental Method X).

2.12. Y-maze test for spatial working memory assessment

Spatial working memory was assessed by the Y-maze test (Supplemental Method XI).

2.13. Statistical analysis

All values are expressed as mean ± standard error of the mean (SEM). One-way analysis of variance was used to evaluate significant differences among groups (except where otherwise stated) followed by a post hoc Tukey test or Tukey-Kramer test. Differences with $p < 0.05$ were considered significant in all statistical analyses.

3. Results

3.1. Mortality rates and body weight changes of rats

The mortality rate in the 2VGO group was 2.0% (1/49). This was much lower than that of the 2VO group, which was 13.8% (8/58), in accordance with previous reports (Fujishima et al., 1976). In the sham group, all 48 rats survived until euthanized. Body weight decreased in both the 2VGO and 2VO groups, which was significantly less severe in the 2VGO group at 1 day postoperation (2VGO group, −14.1 ± 2.0% vs. 2VO group, −27.4 ± 1.7%; $p < 0.01$). Both groups of rats started to regain body weight at 3 days.

3.2. Gradual narrowing of the common carotid arteries

Bilateral placement of the ameroid constrictors on the CCAs produced the expected narrowing of the inner lumen: 0.28 mm at 1 day postoperation, 0.24 mm at 3 days, and 0.19 mm at 5 days (Fig. 1B and C). CTA indicated that blood flow of CCAs distal to the implanted ameroid constrictors did not decrease at 1 hour but started to decrease at 3 hours, leading to complete occlusion of the CCAs at 3 days (Fig. 3).

3.3. Temporal profiles of CBF recorded by LSF

In the 2VO group, CBF dropped sharply to 55.2 ± 0.8% of the baseline level at 3 hours postoperation but started to recover at 3 days and reached to 85.6 ± 3.7% at 28 days. In contrast, in the 2VGO group, the acute phase observed in the 2VO group was absent; CBF did not decrease at 1 hour (102.5 ± 2.9%) but started to decrease at 3 hours (79.6 ± 3.3%), and reached a minimum at 3 days (69.3 ± 1.7%), before gradually recovering at 28 days (84.5 ± 3.3%). In the sham group, no apparent change of CBF was detected. Two-way repeated measures analysis of variance showed a significant interaction between group and time ($F(14,63) = 16.976$; $p < 0.001$) and significant differences between the 2VGO and 2VO groups at 1, 3, and 6 hours, and 1 day (Fig. 4).

The blood pressure and pulse rate of the surviving rats did not differ significantly among the 3 groups at any postoperative intervals until 28 days.

3.4. ^{18}F-FDG PET analysis

The first 5-minute uptake of ^{18}F-FDG, which was used as an indicator of CBF, showed a similar temporal profile of the CBF recorded by LSF: the uptake dropped more sub-

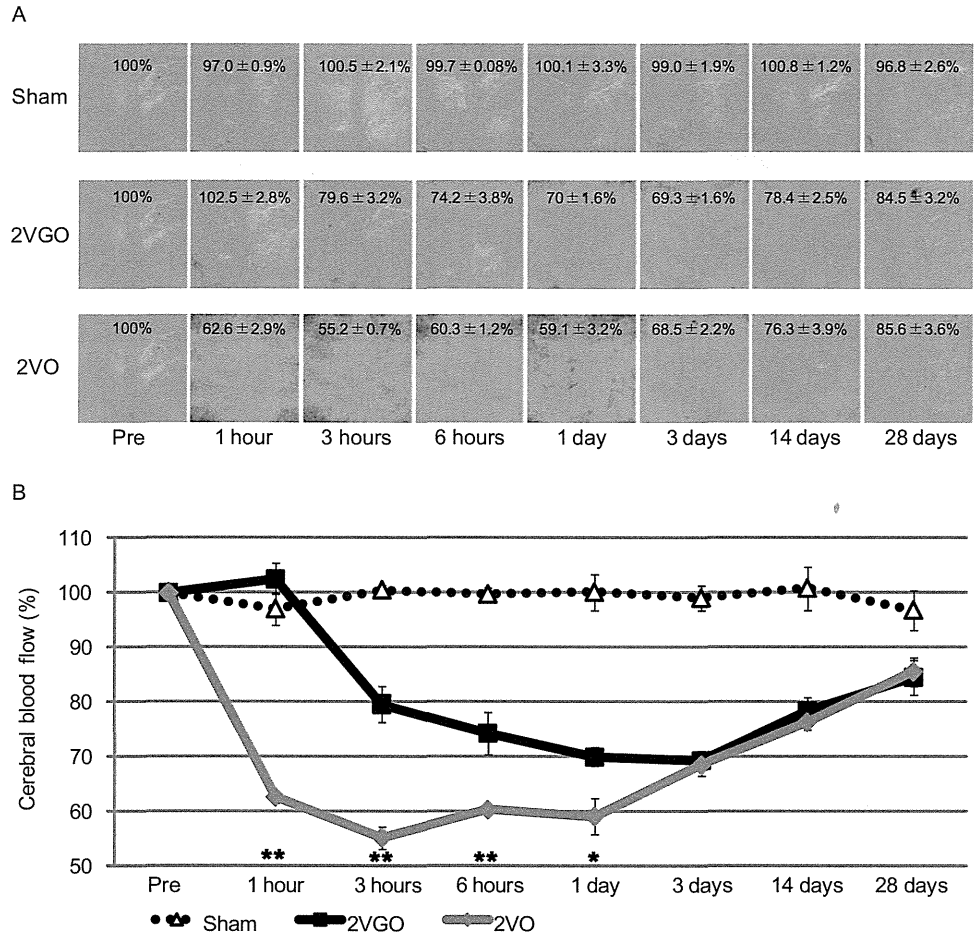

Fig. 4. (A) Representative cerebral blood flow (CBF) images of laser speckle flowmetry in each group at indicated time intervals. The value in each image indicates relative CBF that is expressed as a percentage ± standard error of the mean (SEM) of the baseline level (100%). Four to 6 animals in each group were used at each point. (B) The temporal profile of CBF in each group. * $p < 0.05$, ** $p < 0.01$, 2-vessel gradual occlusion (2VGO) versus 2-vessel occlusion (2VO).

stantially in the 2VO than 2VGO groups at 3 hours postoperation but recovered at 28 days in both groups (Fig. 5A).

The late ^{18}F-FDG uptake, used as an indicator of cerebral glucose metabolism, did not significantly decrease at 28 days in the 2VGO group, whereas in the 2VO group at 28 days, late ^{18}F-FDG uptake significantly decreased in the cerebral cortex compared with that in the 2VGO group and in the hippocampus compared with preoperation (Fig. 5B).

3.5. Y-maze test for spatial working memory assessment

In the 2VGO and 2VO groups, the percentage of alternation behaviors (used as a reflection of spatial working memory) was significantly decreased (Fig. 6A), whereas the number of arm entries was significantly increased, compared with the sham group at 28 days (Fig. 6B).

3.6. Histological analysis of gray matter damage

Brain infarcted areas were not found in any rats of the 2VGO and sham groups but in 50% of rats in the 2VO group at 3, 14, and 28 days (Supplemental Fig. 1A). The infarctions were distributed mainly in the caudoputamen. Cortical gliosis was not found in the sham group and was present in only 8.3% of rats in the 2VGO group at 3, 14, and 28 days (Supplemental Fig. 1B); however, cortical gliosis was present in 75% of rats in the 2VO group over the same periods. There was a trend toward increased density of pyknotic neurons in the hippocampal CA1 region at 28 days in the 2VO group compared with the 2VGO and sham groups (Supplemental Fig. 1C); however, there were no significant differences in density among the 3 groups.

3.7. Histological analysis of white matter damage

Quantitative analysis of the grading score of Klüver-Barrera staining of the corpus callosum indicated that the white matter damage was significantly more severe in both the 2VGO and 2VO groups compared with the sham group at 28 days postoperation; however, the extent of damage was significantly smaller in the 2VGO compared with 2VO groups (Fig. 7A). Similar findings in the degree of myelin damage (assessed by dMBP staining) (Fig. 7B) and the

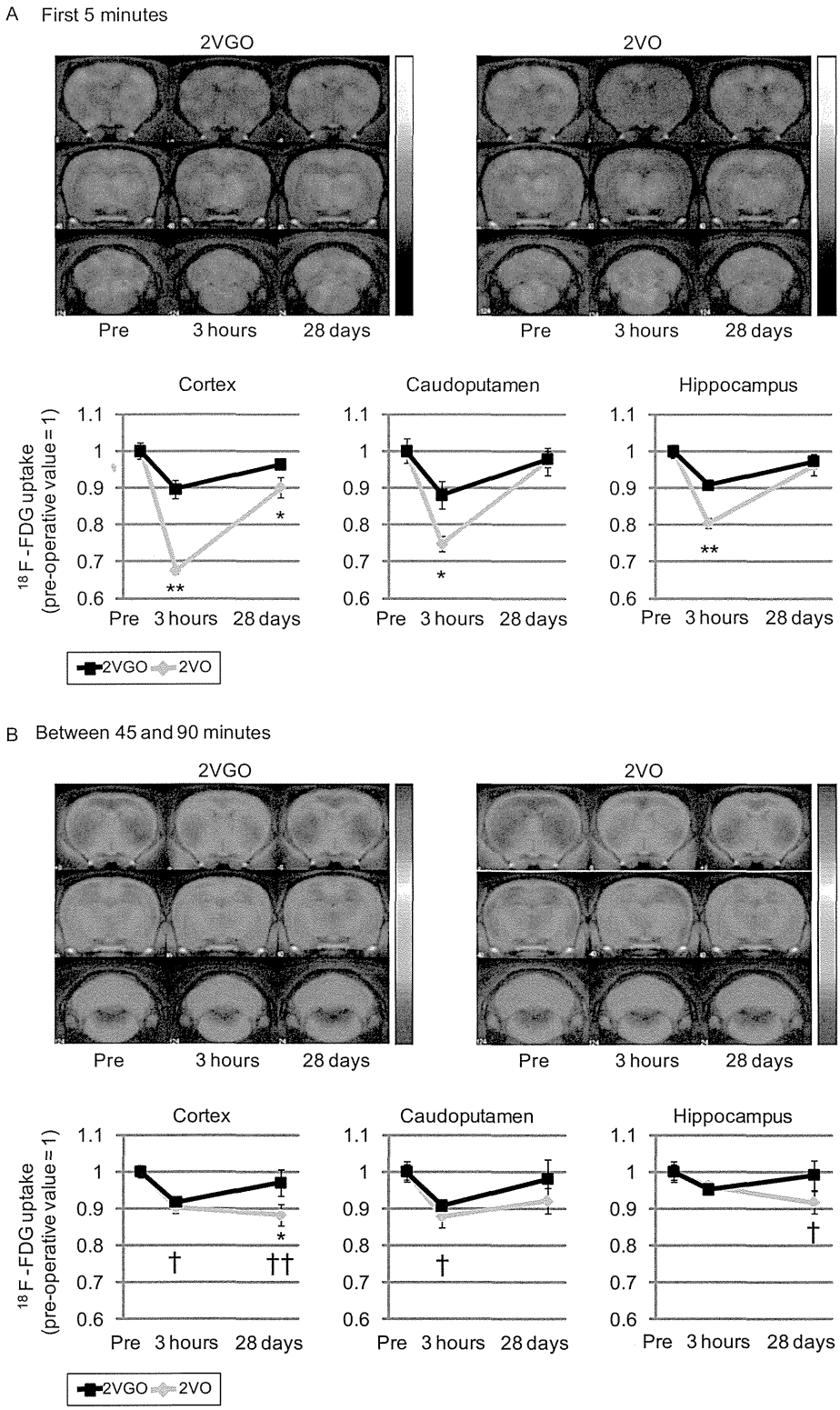

Fig. 5. (A) Representative ^{18}F-fluorodeoxyglucose (FDG) positron emission tomography (PET) coronal images superimposed on magnetic resonance (MR) images for the first 5 minutes of the 2-vessel gradual occlusion (2VGO) (upper left panels) and 2-vessel occlusion (2VO) (upper right panels) groups. Temporal profiles of the mean normalized ^{18}F-FDG count during the first 5 minutes in the cerebral cortex (lower left), caudoputamen (lower middle), and hippocampus (lower right) at indicated time intervals. (B) Representative ^{18}F-FDG PET coronal images superimposed on MR images between 45 and 90 minutes of the 2VGO (upper left panels) and 2VO (upper right panels) groups. Temporal profiles of the mean normalized ^{18}F-FDG count between 45 and 90 minutes in the cerebral cortex (lower left), caudoputamen (lower middle), and hippocampus (lower right) at indicated time intervals. Three to 4 animals in each group were used at each point. * $p < 0.05$; ** $p < 0.01$, 2VGO vs. 2VO. † $p < 0.05$, †† $p < 0.01$, at each period in 2VO group versus preoperation.

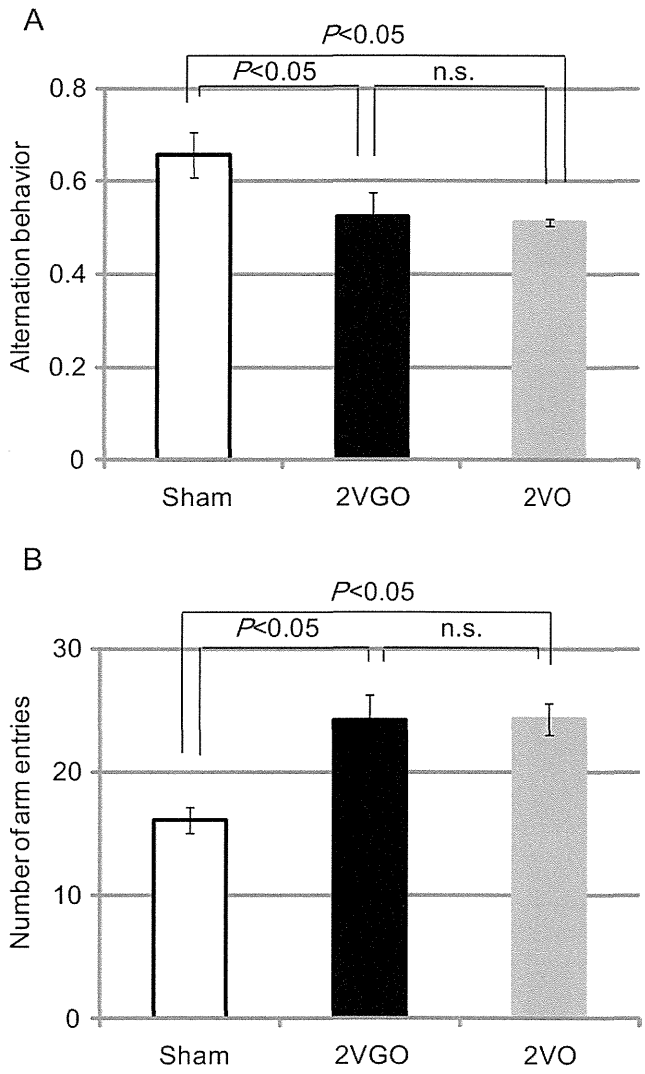

Fig. 6. Histogram showing spatial working memory impairment (A) and the locomotor activity (B) measured by Y-maze test at 28 days postoperation in the sham (n = 10), 2-vessel gradual occlusion (2VGO) (n = 11) and 2-vessel occlusion (2VO) (n = 10) groups.

density of GST-π-positive oligodendrocytes (Fig. 7C) were discovered: the white matter damage was slightly milder in the 2VGO compared with the 2VO groups but was still more severe than the sham group. In the 2VGO and 2VO groups, MAG-immunopositive regions (indicating the degree of axon-glial integrity) decreased compared with the sham group, with the most apparent difference at 28 days (data not shown). The density of glial fibrillary acidic protein-immunopositive astrocytes was significantly greater in both the 2VGO and 2VO groups compared with the sham group at 28 days (data not shown). The density of ionized calcium binding adapter molecule-1-immunopositive microglia increased from 1 day in the 2VO group; while in the 2VGO group, there was no change in microglia density at 1 day but an increase at 3 days. The microglial density in both the 2VGO and 2VO groups remained significantly greater than the sham group at 28 days (Supplemental Fig. 2A and B).

3.8. Western blotting analysis for MBP at 28 days postoperation

In addition to dMBP immunohistochemistry, MBP immunoblotting was evaluated as a marker of white matter integrity. Western blotting for MBP at 28 days showed multiple bands corresponding to the 4 isoforms (21.5/18.5/17/14 kDa). Densitometric analyses showed significant reduction in those bands both in the 2VGO and 2VO groups compared with the sham group. However, the reduction was less substantial in the 2VGO than 2VO groups (Fig. 8).

3.9. mRNA expression of inflammatory cytokines at 1 day postoperation

At 1 day, cerebral mRNA expression of inflammatory cytokines, MCP-1, and TNF-α was significantly increased in the 2VO group but slightly increased in the 2VGO group compared with the sham group (Fig. 9A and B).

3.10. The protein level of TNF-α at 1 day postoperation

At 1 day, cerebral protein level of TNF-α was significantly increased in both the 2VGO and 2VO groups compared with the sham group, with a tendency of increase in the 2VO group (Fig. 9C).

4. Discussion

The findings in this study suggest circumvention of the acute phase of CBF reduction and resultant acute inflammatory response observed in the 2VO model by gradual narrowing of the bilateral CCAs using the ameroid constrictor device instead of ligation. As a result, segregation of the chronic phase from the acute phase was achieved, suggesting a more precise reconstruction of chronic cerebral hypoperfusion evident in clinical cases of SIVD. This method induced demyelinating changes with inflammatory and glial responses but without apparent infarcted lesions or pronounced metabolic derangement in the gray matter. White matter changes were substantial in both the 2VGO and 2VO groups but significantly less severe in the 2VGO group. This suggests that the neuropathological consequences and metabolic changes of the 2VO model had been generated not only by chronic cerebral hypoperfusion but also by acute drop in CBF immediately after bilateral CCAs occlusion. The differences in mortality rate, infarction rate, and body weight loss between the 2VGO and 2VO groups may reflect gradual CBF reduction in the 2VGO group.

Y-maze tests showed significant spatial working memory impairment in both the 2VGO and 2VO groups. The spatial working memory impairment in the 2VGO model may be derived from white matter damage because neuropathological changes and glucose hypometabolism were not apparent in the cortex and hippocampus at 28 days. By contrast,

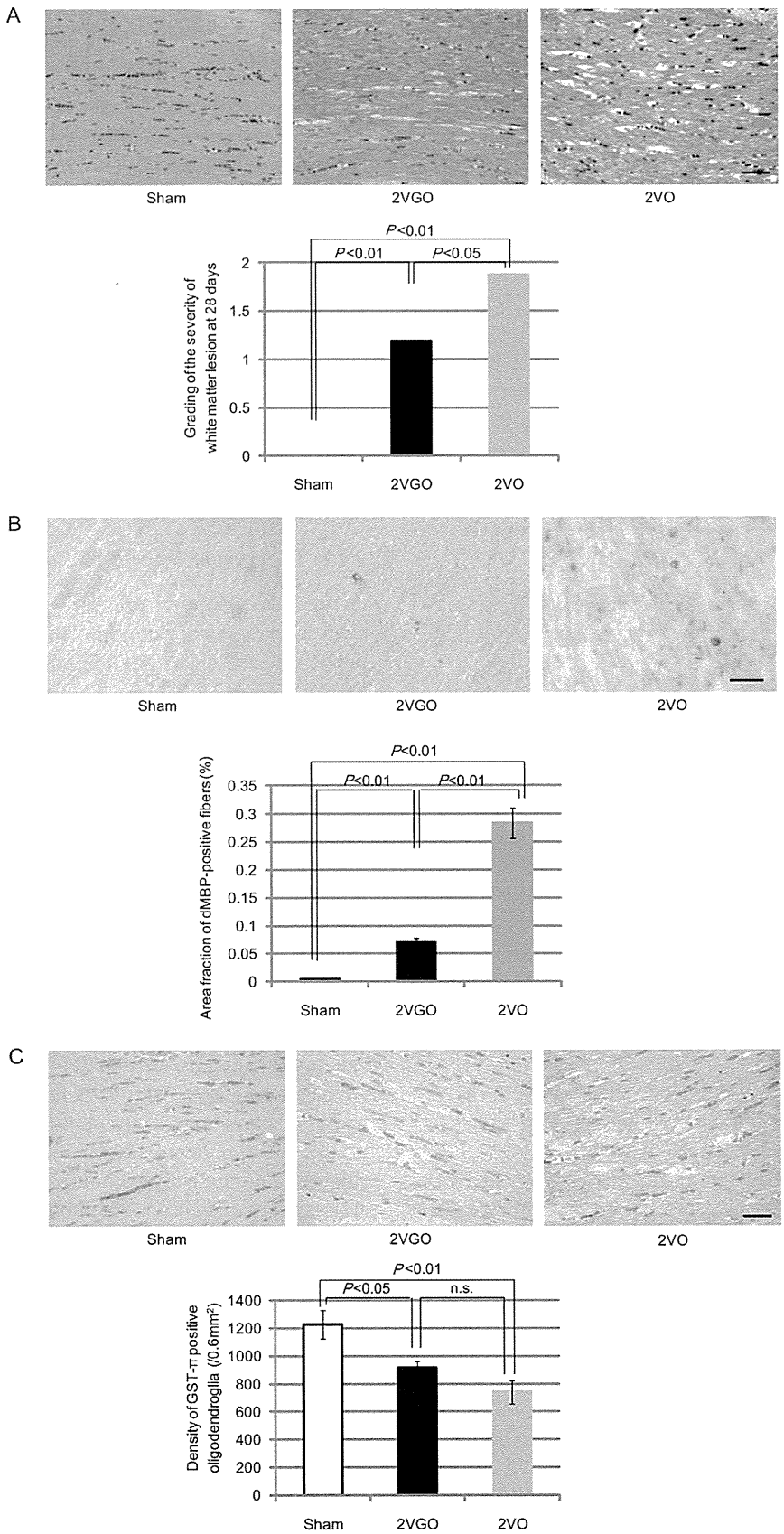
A
Sham
2VGO
2VO
P<0.01
P<0.01
P<0.05
Grading of the severity of white matter lesion at 28 days
2
1.5
1
0.5
0
Sham
2VGO
2VO
B
Sham
2VGO
2VO
P<0.01
P<0.01
P<0.01
Area fraction of dMBP-positive fibers (%)
0.35
0.3
0.25
0.2
0.15
0.1
0.05
0
Sham
2VGO
2VO
C
Sham
2VGO
2VO
P<0.01
P<0.05
n.s.
Density of GST-π positive oligodendroglia (/0.6mm²)
1400
1200
1000
800
600
400
200
0
Sham
2VGO
2VO

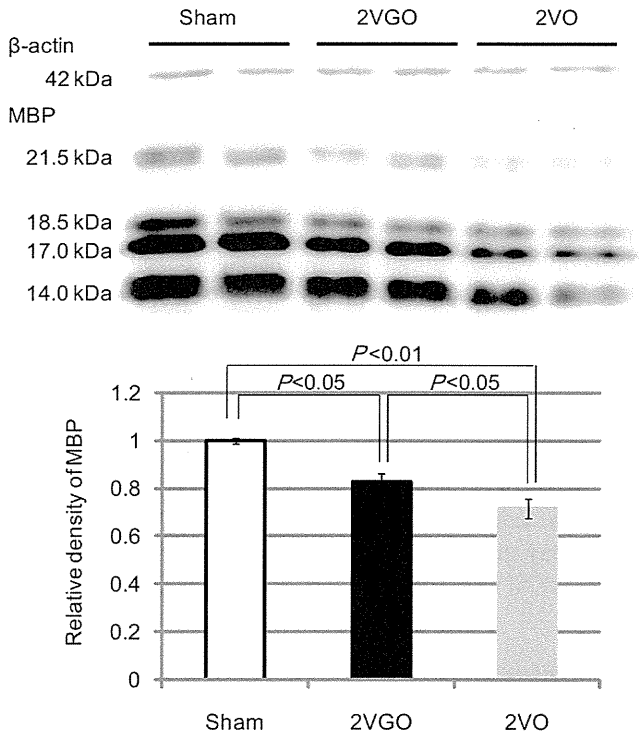

Fig. 8. Representative images of immunoblotting for myelin basic protein (MBP) and β-actin in the optic nerve and chiasma of the sham (n = 4), 2-vessel gradual occlusion (2VGO) (n = 4), and 2-vessel occlusion (2VO) (n = 4) groups at 28 days postoperation. Histogram showing the relative amount of MBP as assessed by densitometric analysis.

the 2VO model exhibited persistent metabolic derangement in the gray matter at 28 days, despite CBF recovery; this suggests neurovascular uncoupling even at 28 days postoperation. The 2VO and 2VGO model may thus be defined by the presence or absence of the acute CBF drop, respectively; therefore, the persistent neurovascular uncoupling at 28 days in the 2VO group may result from the ischemic insult applied to the brain in the acute phase postoperation. These results therefore suggest that the 2VGO model may more closely replicate the condition of working memory impairment subsequent to ischemic white matter changes.

The reasons as to why the 2VGO model showed comparable spatial working memory impairment to the 2VO model may be explained by the fact that less pronounced white matter damage was sustained in the 2VGO model compared with the 2VO model where the damage was sufficient to induce spatial working memory impairment detected by the Y-maze test. Another reason may be the impaired glial-axon integrity (assessed with MAG immunostaining) (Quarles, 2007), which was comparable between 2VGO and 2VO models; this therefore may have contributed to the working memory impairment.

No single animal model appears to recapitulate all the features of SIVD as humans have different brain anatomy and longer perforating arteries. In addition, the current model lacks vascular risk factors and causative small vessel changes that may lead to alterations in blood flow and cerebral autoregulation. One of the ways to resolve this problem could be to implant ameroid constrictors in spontaneous hypertensive rats (SHR) (Lin et al., 2001). However, SHRs subjected to the bilateral CCA occlusion have shown more extensive CBF reduction accompanied by more extensive cerebral infarcts and demyelinating changes and higher mortality rate (72%; 78 of 108) than the corresponding normotensive counterpart WKY rats (16%; 7 of 43) (Fujishima et al., 1976; Ogata et al., 1976). Besides the high mortality, such severe CBF reduction with marked infarctions may not adequately represent SIVD. Our preliminary data showed that the mortality rate of SHRs subjected to implantation of ameroid constrictors to the bilateral CCAs was only 6.2% (1 of 16) (Kitamura, unpublished data). Therefore, comparison of the effects of 2VGO on SHRs and on WKY rats could facilitate our understanding of the clinical and pathological substrates of SIVD with small vessel pathology, with the caveat that the genetic background of SHR is not necessarily identical to that of WKY rats (St. Lezin et al., 1992).

Thus far, rats with several different backgrounds have been used for 2VO model, including Sprague-Dawley, Wistar, and WKY rats. There may therefore have been discrepancies between rats in terms of the temporal CBF profile after 2VO. The relative CBF reduction from the baseline level in the current study was smaller than that found in Sprague-Dawley or Wistar rats but approximated that of WKY rats (Farkas et al., 2007).

The ameroid constrictor has been applied to the porcine or canine coronary arteries to simulate atherosclerotic coronary heart disease (Litvak et al., 1957), and the rabbit and rat femoral arteries to mimic chronic hind limb ischemia (Tang et al., 2005). However, this is the first report that the ameroid constrictor is applied to the CCA to replicate

Fig. 7. (A) Representative images of Klüver-Barrera staining in the corpus callosum at 28 days postoperation in each group (upper panels). Histogram showing the grading of the white matter lesions in the sham (n = 4), 2-vessel gradual occlusion (2VGO) (n = 4), and 2-vessel occlusion (2VO) (n = 4) groups. Scale bar, 50 μm. (B) Representative images of immunohistochemical staining for degraded myelin basic protein (dMBP) in the corpus callosum at 28 days in each group (upper panels). Oligodendrocytic cell bodies of irregular size and myelin sheaths along the axons were densely stained for dMBP. Scale bar, 20 μm. Histogram showing the area fraction (%) of dMBP-immunopositive fibers in the sham (n = 4), 2VGO (n = 4), and 2VO (n = 4) groups. (C) Representative images of the immunohistochemical staining for glutathione S-transferase-pi (GST-π) in the corpus callosum at 28 days in each group (upper panels). Histogram showing the density of GST-π-immunopositive oligodendroglia in the sham (n = 4), 2VGO (n = 4), and 2VO (n = 4) groups. Scale bar, 50 μm.

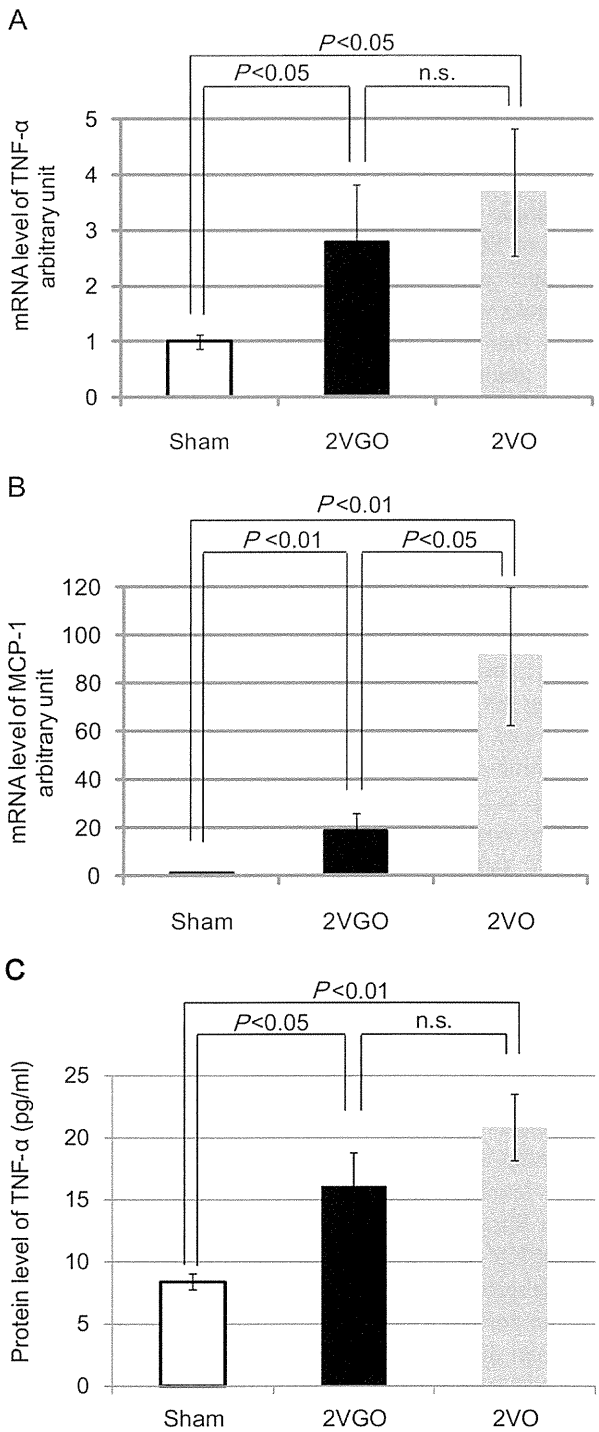

Fig. 9. Histogram showing the messenger RNA levels of tumor necrosis factor-α (TNF-α) (A) and monocyte chemoattractant protein-1 (MCP-1) (B), as analyzed with real-time reverse transcriptase-polymerase chain reaction (RT-PCR), in the right anterior hemisphere of the sham (normalized as 1), 2-vessel gradual occlusion (2VGO) (18.7 ± 7.28 and 2.79 ± 1.02 -fold, respectively), and 2-vessel occlusion (2VO) (91.2 ± 28.8 and 3.68 ± 1.14 -fold, respectively) groups at 1 day postoperation (n = 4 in each group). (C) Histogram showing the protein level of TNF-α, as analyzed with enzyme-linked immunosorbent assay (ELISA), in the left anterior hemisphere of the sham (8.38 ± 0.63), 2VGO (16.0 ± 2.70), and 2VO (20.8 ± 2.67) groups at 1 day postoperation (n = 4 in each group).

chronic cerebral hypoperfusion. Although the ameroid constrictor device achieves predictable gradual narrowing of the artery, the speed of arterial narrowing is dependent on both the size of ameroid constrictor and the diameter of arteries. As such, an in vivo noninvasive imaging technique, such as CTA, may be applicable in the evaluation of the temporal change in carotid blood flow. Moreover, use of titanium for casing, instead of the stainless steel, will enable magnetic resonance imaging/angiography.

Rats of 12–14 weeks of age were used in the current study to reproduce chronic cerebral hypoperfusion. However, application of the ameroid constrictor to older animals for longer periods should be considered given that SIVD is an age-related disease that develops over many years.

In conclusion, we have established a novel rat model that may more closely mimic cognitive impairment subsequent to selective white matter damage. The 2VGO model may therefore be adapted to explore possible treatments for SIVD.

Disclosure statement

The authors disclose no conflicts of interest.

All procedures were performed in accordance with the guidelines for animal experimentation from the ethical committee of Kyoto University.

Acknowledgements

We thank Dr. Matsuo and Dr. Wakita for generously giving us the anti-dMBP antibody, and Dr. Khundakar for insightful comments and editing. We are indebted to Ms. Tanigaki, Ms. Hikawa, Ms. Nakabayashi, Ms. Kawada, Ms. Katsukawa, and Mr. Kubota for their excellent technical assistance. This work was supported by grants from the Suzuken Memorial Foundation (to MI and JT) and the Japanese Vascular Disease Research Foundation (MI). The research work of R.N.K. is supported by the Medical Research Council, UK.

Appendix A. Supplementary data

Supplementary data associated with this article can be found, in the online version, at doi:10.1016/j.neurobiolaging.2011.10.033.

References

Farkas, E., Luiten, P.G., Bari, F., 2007. Permanent, bilateral common carotid artery occlusion in the rat: a model for chronic cerebral hypoperfusion-related neurodegenerative diseases. Brain Res. Rev. 54, 162–180.

Fujishima, M., Ogata, J., Sugi, T., Omae, T., 1976. Mortality and cerebral metabolism after bilateral carotid artery ligation in normotensive and spontaneously hypertensive rats. J. Neurol. Neurosurg. Psychiatry 39, 212–217.

Hainsworth, A.H., Markus, H.S., 2008. Do in vivo experimental models reflect human cerebral small vessel disease? A systematic review. J. Cereb. Blood Flow Metab. 28, 1877–1891.

Ihara, M., Polvikoski, T.M., Hall, R., Slade, J.Y., Perry, R.H., Oakley, A.E., Englund, E., O'Brien, J.T., Ince, P.G., Kalaria, R.N., 2010. Quantification of myelin loss in frontal lobe white matter in vascular dementia, Alzheimer's disease, and dementia with Lewy bodies. Acta Neuropathol. 119, 579–589.

Jiwa, N.S., Garrard, P., Hainsworth, A.H., 2010. Experimental models of vascular dementia and vascular cognitive impairment: a systematic review. J. Neurochem. 115, 814–28.

Lin, J.X., Tomimoto, H., Akiguchi, I., Wakita, H., Shibasaki, H., Horie, R., 2001. White matter lesions and alteration of vascular cell composition in the brain of spontaneously hypertensive rats. Neuroreport 12, 1835–1839.

Litvak, J., Siderides, L.E., Vineberg, A.M., 1957. The experimental production of coronary artery insufficiency and occlusion. Am. Heart J. 53, 505–518.

Marosi, M., Rákos, G., Robotka, H., Németh, H., Sas, K., Kis, Z., Farkas, T., Lür, G., Vécsei, L., Toldi, J., 2006. Hippocampal (CA1) activities in Wistar rats from different vendors. Fundamental differences in acute ischemia. J. Neurosci. Methods 156, 231–235.

Marshall, R.S., Lazar, R.M., 2011. Pumps, aqueducts, and drought management: vascular physiology in vascular cognitive impairment. Stroke 42, 221–226.

Ogata, J., Fujishima, M., Morotomi, Y., Omae, T., 1976. Cerebral infarction following bilateral carotid artery ligation in normotensive and spontaneously hypertensive rats: a pathological study. Stroke 7, 54–60.

Otori, T., Katsumata, T., Muramatsu, H., Kashiwagi, F., Katayama, Y., Terashi, A., 2003. Long-term measurement of cerebral blood flow and metabolism in a rat chronic hypoperfusion model. Clin. Exp. Pharmacol. Physiol. 30, 266–272.

Pantoni, L., 2010. Cerebral small vessel disease: from pathogenesis and clinical characteristics to therapeutic challenges. Lancet Neurol. 9, 689–701.

Quarles, R.H., 2007. Myelin-associated glycoprotein (MAG): past, present and beyond. J. Neurochem. 100, 1431–1448.

Shibata, M., Ohtani, R., Ihara, M., Tomimoto, H., 2004. White matter lesions and glial activation in a novel mouse model of chronic cerebral hypoperfusion. Stroke 35, 2598–2603.

St. Lezin, E., Simonet, L., Pravenec, M., Kurtz, T.W., 1992. Hypertensive strains and normotensive "control" strains. How closely are they related? Hypertension 19, 419–424.

Tang, G.L., Chang, D.S., Sarkar, R., Wang, R., Messina, L.M., 2005. The effect of gradual or acute arterial occlusion on skeletal muscle blood flow, arteriogenesis, and inflammation in rat hindlimb ischemia. J. Vasc. Surg. 41, 312–320.

Tomimoto, H., Ihara, M., Wakita, H., Ohtani, R., Lin, J.X., Akiguchi, I., Kinoshita, M., Shibasaki, H., 2003. Chronic cerebral hypoperfusion induces white matter lesions and loss of oligodendroglia with DNA fragmentation in the rat. Acta Neuropathol. 106, 527–534.

Wakita, H., Tomimoto, H., Akiguchi, I., Kimura, J., 1994. Glial activation and white matter changes in the rat brain induced by chronic cerebral hypoperfusion: an immunohistochemical study. Acta Neuropathol. 87, 484–492.

Wakita, H., Tomimoto, H., Akiguchi, I., Matsuo, A., Lin, J.X., Ihara, M., McGeer, P.L., 2002. Axonal damage and demyelination in the white matter after chronic cerebral hypoperfusion in the rat. Brain Res. 924, 63–70.

Yoshitake, T., Kiyohara, Y., Kato, I., Ohmura, T., Iwamoto, H., Nakayama, K., Ohmori, S., Nomiyama, K., Kawano, H., Ueda, K., et al., 1995. Incidence and risk factors of vascular dementia and Alzheimer's disease in a defined elderly Japanese population: the Hisayama Study. Neurology 45, 1161–1168.

Yoshizaki, K., Adachi, K., Kataoka, S., Watanabe, A., Tabira, T., Takahashi, K., Wakita, H., 2008. Chronic cerebral hypoperfusion induced by right unilateral common carotid artery occlusion causes delayed white matter lesions and cognitive impairment in adult mice. Exp. Neurol. 210, 585–591.